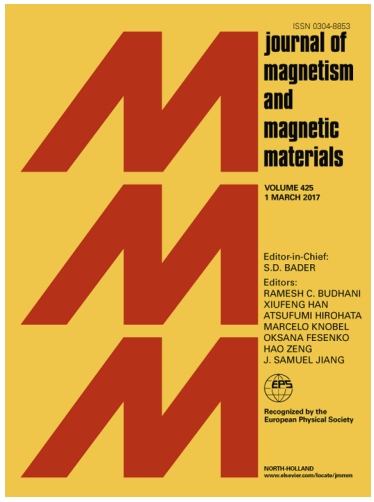

Tuning the ferromagnetism of epitaxial-strained $D0_{19}$-Mn_3Ga thin films

José T. Holguín-Momaca, Christian J. Muñoz-Carnero, Himanshu Sharma, Carlos R. Santillán-Rodríguez, José A. Matutes-Aquino, C.V. Tomy, Sion F. Olive-Méndez

PII: S0304-8853(18)32350-3
DOI: https://doi.org/10.1016/j.jmmm.2018.09.100
Reference: MAGMA 64382

To appear in: *Journal of Magnetism and Magnetic Materials*

Received Date: 26 July 2018
Revised Date: 27 August 2018
Accepted Date: 26 September 2018

Please cite this article as: J.T. Holguín-Momaca, C.J. Muñoz-Carnero, H. Sharma, C.R. Santillán-Rodríguez, J.A. Matutes-Aquino, C.V. Tomy, S.F. Olive-Méndez, Tuning the ferromagnetism of epitaxial-strained $D0_{19}$-Mn_3Ga thin films, *Journal of Magnetism and Magnetic Materials* (2018), doi: https://doi.org/10.1016/j.jmmm.2018.09.100

Tuning the ferromagnetism of epitaxial-strained $D0_{19}$-Mn_3Ga thin films

José T. Holguín-Momaca[a], Christian J. Muñoz-Carnero[a], Himanshu Sharma[b], Carlos R. Santillán-Rodríguez[a], José A. Matutes-Aquino[a], C. V. Tomy[c], and Sion F. Olive-Méndez[a,*]

[a] *Centro de Investigación en Materiales Avanzados, S.C. (CIMAV), Miguel de Cervantes No. 120, C.P. 31136, Chihuahua, Chih., México.*

[b] *Institute for Materials Research, Tohoku University, Sendai 980-8577, Japan.*

[c] *Department of Physics, Indian Institute of Technology Bombay, Powai, Mumbai - 400 076, India.*

Abstract

The hexagonal $D0_{19}$-Mn_3Ga phase is a non-collinear antiferromagnet with a triangular spin configuration. The Mn magnetic moments, lying in the (001) basal plane, are slightly canted towards the *c* axis producing a ferromagnetic component (FMC), which saturation magnetization in bulk samples is 7.7 kAm^{-1}. Here, we report on the epitaxial growth of Mn_3Ga epitaxial thin films on MgO(111), GaN(001) and MgO(001)/Pt(111) substrates with lattices mismatches of -4.77%, 2.1%, and 2.45%, respectively. Structural characterization with reflection high-energy electron diffraction was used to evaluate the critical thicknesses at which relaxation is reached. We provide evidence of the manipulation of the magnitude of the FMC of the Mn_3Ga thin films grown under tensile and compressive deformations. The FMC has been tuned from 23.7 to 11.8 and 2.5 kAm^{-1} for the growth of Mn_3Ga on MgO(111), GaN(001), and MgO(001)/Pt(111) substrates. The modulation of the FMC is explained in terms of the Dzyaloshinskii-Moriya interaction.

Keywords: Non-collinear antiferromagnet; ferromagnetic; $D0_{19}$-Mn_3Ga; epitaxial thin film; deformation

E-mail: sion.olive@cimav.edu.mx

1. Introduction

A promising material for the elaboration of spintronic devices due to the unique combination of magnetic and structural properties is Mn_3Ga [1,2,3], which possesses three crystalline structures: cubic, tetragonal, and hexagonal. The cubic phase $L2_1$-Mn_3Ga is a metastable antiferromagnetic (AFM) compound, obtained usually by spin melting [4]. The tetragonal $D0_{22}$-Mn_3Ga phase is ferrimagnetic and is a potential candidate to elaborate the free layer of magnetic tunnel junctions (MTJ) where the switching of the free layer can be achieved by the spin-torque transfer process [5,6]. Bulk $D0_{22}$-Mn_3Ga can be easily obtained by arc melting stoichiometric amounts of Ga and Mn. Further annealing of $D0_{22}$-Mn_3Ga pellets at 400 °C for 1-2 weeks produces the nucleation and formation of the $D0_{19}$ phase [7]. The hexagonal $D0_{19}$-Mn_3Ga (Mn_3Ga), space group $P6_3/mmc$, is AFM and it has been used to produce exchange bias on $Co_{50}Fe_{50}$ layers [8] and tested in CoFeB/MgO-based MTJ reaching a tunneling magnetoresistance of ~160% at room temperature [9]. In the form of thin films Mn_3Ga can be grown at 400 °C under the influence of an hexagonal seed layer as Ru. The hexagonal crystalline structure of Mn_3Ga is constituted by the atomic position, Mn: 2c(⅓,⅔,¼) and Ga: 6h(x,2x,¼) with x = ⅚, and lattice parameters a = 5.404 Å and c = 4.353 Å. The magnetic moments of the Mn atoms have a triangular spin configuration in the (001) basal plane [7] and the Néel temperature, T_N, of the compound is 470 K [10]. The triangular arrangement of the Mn magnetic moments are located at z = ¼ and z = ¾ and the chirality of the triangular spin configuration is opposite from one plane to another as shown in Fig. 1(a) and the top view in Fig. 1(b). The magnetic moments of Mn atoms are slightly canted out-of-plane (OP) towards the c axis producing a ferromagnetic component (FMC) [11], which has been experimentally measured to be 7.7 kAm^{-1} (0.045μ_B/fu) [4] and theoretically calculated to be 5.1 kAm^{-1} (0.03μ_B/fu) [12]. Similar spin configuration, with a vertical canting of the Mn magnetic moments has been observed on the isostructural Mn_3Sn and Mn_3Ge compounds where the magnetic moments of the FMCs per formula unit are 0.009μ_B [13] and 0.06μ_B [14], respectively. Nagamiya *et al.* suggested that one of the three spins is parallel to a local crystallographic direction, which behaves as the *spin axis*, and that the adjacent Mn atoms are canted towards the *spin axis* and relaxed through the Dzyaloshinskii-Moriya interaction thus producing the FMC [15].

In this paper we report on the manipulation of the FMC of $D0_{19}$ Mn_3Ga epitaxial thin films grown on MgO(111), GaN(001) and MgO(001)/Pt(111) substrates using magnetron sputtering technique. The different lattice mismatch between the substrates and the Mn_3Ga layers induce tensile/compressive deformation thus tuning the Mn-Mn interatomic distances reducing/increasing the canting of the magnetic moments of the Mn atoms.

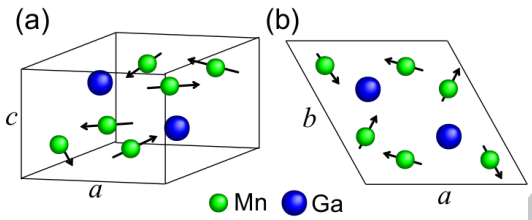

Figure 1. (a) Crystalline structure of Mn_3Ga and (b) top-view along the [001] direction.

2. Experiment

The growth of the epitaxial thin films was performed using radio-frequency magnetron sputtering technique. The base pressure of the growth chamber is better than 5×10^{-8} Torr and thin film growth was achieved at 3 mTorr. The films were obtained from a homemade Mn_3Ga target eroded at 55 W. The deposition rate is 3.4 nm/min. Thin film growth was achieved at different substrate temperatures, T_s, of 400, 500 and 600 °C, but only T_s = 400 °C leads to the formation of the $D0_{19}$ phase, higher temperatures lead to the formation of the $D0_{22}$ crystalline structure despite the influence of the hexagonal symmetry from the substrates. The layers were structurally characterized using a reflection high-energy electron diffraction (RHEED) equipment from STAIB operating at 30 kV, integrated into the sputtering growth chamber with a differential pumping system. RHEED was used to measure the lattice constant evolution with the thickness of the thin films. Phase identification of the $D0_{19}$ crystalline structure was carried out by X-ray diffractometry (XRD) with a PANalytical X'Pert equipment. Magnetic measurements were systematically performed using a physical properties measuring system (PPMS) with an applied magnetic field of 9 T and in a superconducting quantum interference device (SQUID) with an applied field of 0.5 T, both from Quantum Design.

3. Results and discussion

The selection of MgO(111), GaN(001) and MgO(001)/Pt(111) substrates for the growth of the Mn_3Ga layers was based on the lattice mismatch with Mn_3Ga, which may induce tensile/compressive deformations near the interface with the substrate. To calculate the lattice mismatch we used the expression $\Delta a/a = (a_{sub} - a_{film})/a_{sub} \times 100$, where a_{sub} and a_{film} are the lattice constants of the periodicity at the surface of the substrate and that of the film (the in-plane lattice parameter of the $D0_{19}$-Mn_3Ga is a_{Mn3Ga} = 5.404 Å). The crystalline structure of MgO, NaCl-type, has a lattice parameter a = 4.212 Å. The surface of a MgO(111) oriented substrate has an in-plane lattice parameter a = 5.158 Å, hence the lattice mismatch $\Delta a/a$ = -4.77%, indicating that the film may grow under a high in-plane (IP) compressive strain. Ga-terminated GaN(001) substrates, with hexagonal (wurtzite) crystal structure, are commercial template layers grown on Si(111)/AlN substrates. The lattice parameters are a = 3.187 Å and c = 5.186 Å, the match with the film is reached within a rotation of 30° of the Mn_3Ga cell related to the unit cell of GaN(001), thus $a_{Mn3Ga} \sim \sqrt{3} a_{GaN}$ and $\Delta a/a$ = 2.1%, the positive sign indicates the film may be subjected to tensile IP deformation at the interface. Finally, the Pt buffer layer with (111) orientation has been epitaxially grown on MgO(001) substrates at T_s = 200 °C; T_s > 500 °C leads to a change on the epitaxial relationship: MgO(001)‖Pt(001) [16]. Pt has a fcc crystal structure with lattice parameter a = 3.92 Å, the lattice constant of the hexagonal periodicity of two cells on the (111) facet is 5.54 Å, hence $\Delta a/a$ = 2.45%. This lattice mismatch is scarcely larger than that calculated from the lattice constant of GaN(001) substrate but with significant effects on the modulation of the FMC as it will be shown later. The data of the lattice constants, the lattice mismatches, and saturation magnetizations, M_s, of the FMC are summarized in table 1.

Figures 2(a)-2(c) shows the RHEED patterns recorded in real time during the thin film growth. The first row corresponds to the RHEED patterns of the selected substrates along equivalent azimuths where the lattice constants are similar and before the thin film deposition: (a) MgO(111), (b) GaN(001) and (c) MgO(001)/Pt(111). The RMS (root mean square) roughness of the substrate surface is better than 10 Å. The second and third rows are the RHEED patterns of the Mn_3Ga layers at two different thicknesses: 1 and 50 nm.

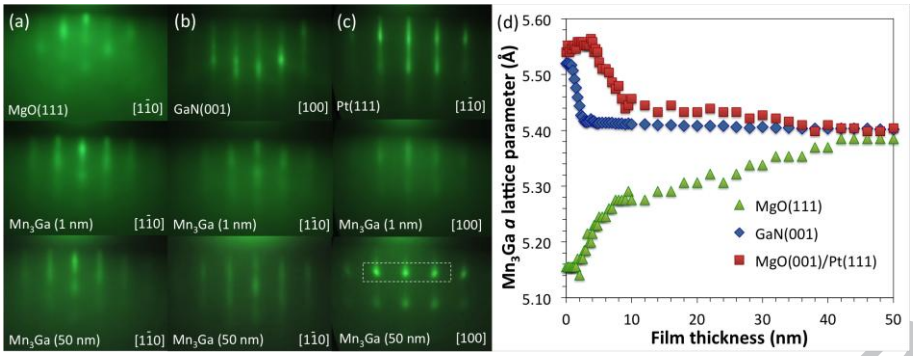

Fig. 2. RHEED diffraction patterns of monocrystalline substrates: (a) MgO(111), (b) GaN(001) and (c) MgO(001)/Pt(111) (first row). Subsequent RHEED patterns of Mn_3Ga deposition at different thicknesses: 1 and 50 nm (second and third rows, respectively). (d) The evolution of the relaxation of the films grown on each substrate.

At the initial growth steps of Mn_3Ga (RHEED pattern shown for a thickness of 1 nm) a wetting layer covering the substrate surface leads to the formation of streaky patterns, typical of smooth surfaces despite the lattice mismatches. As the thickness of the Mn_3Ga layers increases, the RHEED pattern turns progressively into a 3-dimensional spotty pattern indicating an increase of the surface roughnes, but maintaining the monocrystalline microstructure of the film. This characteristic can be observed in the RHEED pattern of the film grown on MgO(001)/Pt(111). In all cases, the layers are epitaxial with the (001) plane of Mn_3Ga parallel to the plane of the film. From the RHEED patterns, we have measured the deformation of the *a* lattice constant of Mn_3Ga at the growth front from a line profile scan in the region indicated at the bottom of Fig. 2(c). The evolution of the streak separation, corresponding to the lattice parameter a^* in the reciprocal space, has been converted to the direct space using as a reference the lattice constant of the substrates. This measuring process was performed for all the films and is shown in Fig. 2(d). The critical thicknesses at which relaxation is reached are 40, 3 and 10 nm for the growth on MgO(111), GaN(001) and MgO(001)/Pt(111), respectively. The plots in Fig. 2(d) indicate that the films are completely relaxed for a thickness of 50 nm. The induced deformation from the substrate has a strong influence at the initial growth steps, (i.e., a few nanometers from the interface). The induced deformation along two perpendicular directions, measured

by RHEED, is equal (results not shown for the perpendicular directions). The fact that the Mn_3Ga thin film grown on MgO(111) reaches relaxation at a higher thickness than those grown in MgO(001)/Pt(111) and GaN(001) substrates, can be explained in terms of the growth mode: the formation of nanoislands after the formation of a wetting layer (Stranski-Krastanov growth mode) allows a faster relaxation than that of a bi-dimensional growth expected from the use of MgO(111) substrates.

The construction of a $(\sqrt{3}\times\sqrt{3})R30°$ cell at the surface of the MgO(111) and GaN(001) substrates is necessary to reach the lattice matching of Mn_3Ga within a $\Delta a/a$ of -4.76% and 2.45%, respectively. Usually, $\Delta a/a$ should be less than ~4% to ensure epitaxial growth. However, successfully monocrystalline growth has been achieved even on MgO(111) substrates where $\Delta a/a$=-4.76%. A similar construction is necessary for the (111) plane of the Pt buffer layer; in this case a (2×2) supercell matches a single Mn_3Ga cell within the corresponding lattice mismatch.

To confirm the formation of the $D0_{19}$ phase, XRD patterns of all samples were obtained in Bragg-Brentano configuration and are shown in Fig. 3. The XRD patterns only indicate the presence of the (002) peak, which in turn confirms that the (002) plane is parallel to the film plane confirming the epitaxial growth described by the RHEED patterns. The dotted line represents the position at 41.45° at which the (002) peak of relaxed samples may be found [17]. The shift of the peaks towards high angles indicates lattice compression along the [001] direction, which is the case of the sample grown on MgO(001)/Pt(111), while the shift towards lower angles implies a lattice expansion (i.e., an IP compressive deformation).

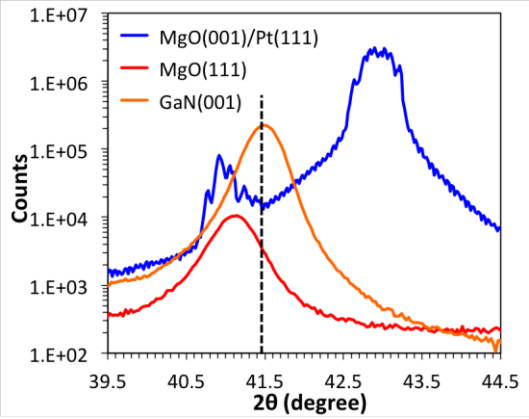

Fig. 3. (a) XRD diffraction patterns of 50 nm-thick $D0_{19}$-Mn_3Ga thin films grown on the selected substrates showing the (002) peak.

The aim of this work is to manipulate and quantify the intrinsic FMC along the *c* axis of the Mn_3Ga layers grown under different induced deformations. For this purpose, IP and OP magnetic *M-H* measurements were performed at 300 K in PPMS and SQUID magnetometers with maximum applied fields of 9 and 0.5 T, respectively. The obtained loops after the subtraction of the diamagnetic components from the substrates (from the *M-H* measurements of bare substrates) are shown in Figs. 4(a)-4(c). In all samples, saturation magnetization, M_s, is reached at ~5 T. It is important to note that M_s is not the same on the IP and OP loops, this effect could be attributed to the induced deformation of the film near the interface or to the effect of shape anisotropy of single AFM domains. In all cases, M_s is $\leq$ 200 kAm^{-1}, which corresponds to a magnetic moment of 1.16 μ_B/f.u., this low value implies that spin flop during the magnetization process leads to AFM (antiparallel) arrangement of two Mn sublattices with a null contribution to the total magnetization of the samples. It has been reported that the magnetic moment per Mn atom at room temperature of the $D0_{19}$ phase in form of thin films is 2.4 μ_B [9] and also that the triangular spin configuration is free to rotate under the application of magnetic fields [18]. Thus, in the IP magnetization process, AFM coupling can not be discarded as saturation is reached in two different steps identified by two different linear magnetic field dependences on the magnetization: the interval from 0 to 0.5 T and the interval from 0.5 to 5 T in the IP curves in Figs. 4(a) to 4(c). The transition between two different magnetization rates (i.e., at 0.5 T) can be interpreted as the spin flop of the magnetic orientation of one of the Mn sublattices to set AFM coupling with another sublattice. For the OP *M-H* measurements the linear magnetic field dependence on the magnetization at fields < 5 T (except for the step at the origin, which corresponds to the FMC) corresponds to an AFM behavior measured perpendicular to a spin axis. However, is important to note that such spin axis does not exist, but that one single spin aligned with an applied magnetic field can behave as the spin axis [15]. In other words, the spin axis will be that direction in which the magnetic field is applied. This fact is confirmed by *M-H* measurements performed along different azimuths of the samples (at 45° and 90° with the current measurements, not shown); the shape of the

IP *M-H* curves remain unchanged. To further obtain accurate information about the behavior of the magnetization at low magnetic fields, SQUID *M-H* loops with a maximum applied magnetic field of 0.5 T were performed and overlapped to the PPMS *M-H* curves as shown in Figs. 4(a)-4(c).

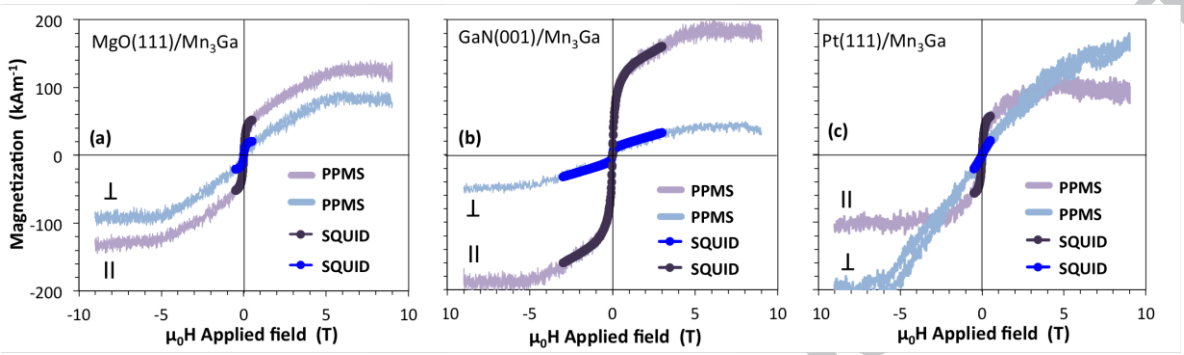

Fig. 4. In-plane and out-of-plane PPMS *M-H* loops at high magnetic fields and SQUID loops at low magnetic fields of 50 nm-thick Mn_3Ga thin films grown on (a) MgO(111), (b) GaN(001), and (c) MgO(001)/Pt(111) substrates.

The net FMC of the thin films are obtained from the SQUID OP curves after the subtraction of a linear fit matching the slope of the AFM component in the magnetic field range -5 T $\leq H \leq$ 5 T as shown in Fig. 5(a). The M_s of the FMC for the films grown on MgO(111), GaN(001) and MgO(001)/Pt(111) substrates are 23.7, 11.8, and 2.5 kAm^{-1}, which correspond to 0.138, 0.069 and 0.014 μ_B/f.u., respectively. The results are summarized in table 1. A clear effect of the compressive/tensile deformation can be observed. Similar IP and OP loops were obtained on Mn_3Sn thin films with a clear signature of the FMC [19]. The triangular spin configuration of the hexagonal structure of Mn_3Ga lacks a defined spin axis along to which the magnetic sublattices may be aligned; instead, three sublattices are oriented at 120° from each other, the direction of each spin can be considered as an individual spin axis. The non-collinear exchange interaction of two adjacent, non-parallel, spin vectors is described by the Dzyaloshinskii-Moriya interaction $H_{DM} = D_{ij} \cdot (S_i \times S_j)$. In the triangular spin configuration of Mn_3Ga (and isostructural compounds) the minimization of the total energy in the cell requires the spin canting along the *c*-axis [20] decreasing the relative angle between each Mn magnetic moment and thus decreasing the

factor $(S_i \times S_j)$. The magnitude of the Dzyaloshinskii-Moriya interaction, $D_{ij} \cdot (S_i \times S_j)$, decreases as well. As a consequence, a rapprochement of the Mn atoms promotes the canting of the Mn-magnetic moments. On the other hand, the increase of the interatomic distances implies the reduction of the canting and thus a reduction of the FMC.

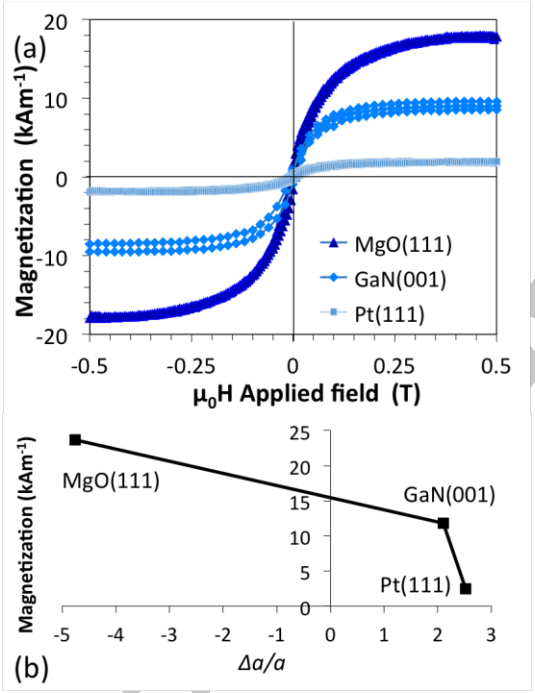

Fig. 5. (b) Ferromagnetic components subtracted from the region centered at the origin of the curves in Fig. 4 obtained from SQUID experiments. (b) Values of the modulation of the FMC vs. lattice mismatch.

Table 1. Lattice parameters a of the used substrates (a_{Mn3Ga} = 5.404 Å); lattice mismatch $\Delta a/a$, and the magnetization of the FMC of Mn_3Ga thin films grown on the selected substrates.

Substrate	a (Å)	$\Delta a/a$ (%)	M_s (kAm^{-1})
MgO(111)	4.21	-4.77	23.7
GaN(001)	3.16	2.1	11.8
MgO(001)/Pt(111)	3.92	2.45	2.5

A similarr effect on the canting of the spin on Mn atoms has been theoretically calculated on Mn_5Ge_3 compound submitted to compressive deformation [21]. In this system a contraction of the hexagonal cell leads to an alignment of the Mn magnetic moments. The minimum FMC magnetization observed on the MgO(001)/Pt(111)/Mn_3Ga system, is 2.5 kAm^{-1}, which corresponds to a magnetic moment of 0.0138 μ_B/f.u., about ⅓ of the experimental 0.045 μ_B/f.u. value measured on bulk samples [7]. The dependence of the M_s on the lattice mismatch is shown in Fig. 5(b). It can be noticed that a slight change in the tensile deformation from the selection of the GaN(001) substrate to the Pt(111) buffer layer reduces the FMC drastically.

4. Conclusions

We have grown epitaxial thin films of the hexagonal $D0_{19}$ phase of Mn_3Ga on MgO(111), GaN(001), and MgO(001)/Pt(111) substrates. Tensile and compressive deformations, measured from RHEED patterns, were induced due to the lattice mismatches between film and substrate. In-plane M-H magnetic measurements have been used to examine the behavior of the triangular configuration of the Mn magnetic moments. The ferromagnetic component of the Mn_3Ga thin films has been tuned acquiring the values of 23.7, 11.8, and 2.5 kAm^{-1}, for the effect of the lattice mismatch of the growth on MgO(111), GaN(001) and MgO(001)/Pt(111) substrates, respectively.

Acknowledgments

The authors thank the financial support received from the Air-Force Office of Scientific Research (AFOSR) and Army Research Laboratory (ARL) Grant No. W911NF-13-1-0177. They also appreciate the facilities provided by Laboratorio Nacional de Nanotecnología-CIMAV.

References

[1] Z H, Zhang Y J, Liu G D, Ding B, Liu E K, Jafri H M, Hou Z P, Wang W H, Ma X Q, Wu G H, 2017, Transition from anomalous hall effect to topological hall effect in hexagonal non-collinear magnet Mn_3Ga, Sci. Rep. 7 (2017) 515.

[2] W.Y. Zhang, P. Kharel, S. Valloppilly, R. Skomski and D.J. Sellmyer, Synthesis and magnetism of single-phase Mn-Ga films, J. Appl. Phys. 117 (2015) 17E306.

[3] O. Akdogan, Synthesis of hard magnetic Mn_3Ga micro-islands by e-beam evaporation, AIP Advances 8 (2018) 056716.

[4] P. Kharel, Y. Huh, N. Al-Aqtash, V.R. Shah, R.F. Sabirianov, R. Skomski and D.J. Sellmyer, Structural and magnetic transitions in cubic Mn_3Ga. J. Phys.: Condens. Matter 26 (2014) 126001.

[5] R.M. Gutiérrez-Pérez, J.T. Holguín-Momaca, J.T. Elizalde-Galindo, F. Espinosa-Magaña and S.F. Olive-Méndez, Giant magnetization on Mn_3Ga ultra-thin films grown by magnetron sputtering on SiO_2/Si(001) J. Appl. Phys. 117 (2015) 123902.

[6] R. M. Gutiérrez-Pérez, R. López Antón, K. Załęski, J. T. Holguín-Momaca, F. Espinosa-Magaña, S. F. Olive-Méndez, Tailoring magnetization and anisotropy of tetragonal Mn_3Ga thin films by strain-induced growth andspin-orbitt coupling, Intermetallics 92 (2018) 20-24.

[7] E. Krén and G. Kádár, Neutron diffraction study of Mn_3Ga Solid State Commun. 8(20) (1970) 1653.

[8] H. Wu, I. Sudoh, R. Xu, W. Si, C.A.F. Vaz, J.-Y. Kim, G. Vallejo-Fernandez and A. Hirohata, Large exchange bias induced by polycrystalline Mn3Ga antiferromagnetic films with controlled layer thickness, J. Phys. D: Appl. Phys. 51 (2018) 215003.

[9] H. Kurt, K. Rode, H. Tokuc, P. Stamenov, M. Venkatesan and J.M.D Coey, Exchange-biased magnetic tunnel junctions with antiferromagnetic ε-Mn_3Ga Appl. Phys. Lett. 101 (2012) 232402

[10] H. Kurt, K. Rode, M. Venkatesan, P. Stamenov and J.M.D. Coey, $Mn_{3-x}Ga(0<x<1)$: Multifunctional thin film materials for spintronics and magnetic recording. Phys. Status Solidi B 248(10) (2011) 2338-2344.

[11] S. Tomiyoshi, Y. Yamaguchi, Triangular spin configuration and weak ferromagnetism of Mn_3Ge J. Mag. Mag. Mater. 31–34(2) (1983) 629–630.

[12] D. Zhang, B. Yan, S.-C. Wu, J. Kübler, G. Kreiner, S.S.P. Parkin and C. Felser, First-principles study of the structural stability of cubic, tetragonal and hexagonal phases in Mn_3Z (Z=Ga, S, and Ge) Heusler compounds, J. Phys.: Condens. Matter 25 (2013) 206006.

[13] P.J. Brown, V. Nunez, F. Tasset, J.B. Forsyth and P. Radhakrishna, Determination of the magnetic structure of Mn_3Sn using generalized neutron polarization analysis J. Phys. Condens. Matter 2 (1990) 9409–9422.

[14] G. Kádár and E. Krén, Neutron diffraction study of Mn_3Ge, Int. J. Magn. 1 (1971) 143.

[15] T. Nagamiya, S. Tomiyoshi and Y. Yamaguchi, Triangular spin configuration and weak ferromagnetism of Mn_3Sn and Mn_3Ge Solid State Commun. 42 (1982) 385–388.

[16] K.H. Ahn, S. Baik and S.S. Kim, Change of growth orientation in Pt films epitaxially grown on MgO(001) substrates by sputtering J. Mater. Res. 17(9) (2002) 2334-2338.

[17] F. Hu, G. Xu, Y. You, Z. Zhang, Z. Xu, Y. Gong, E. Liu, H. Zhang, E. Liu, W. Wang and F. Xu, Tunable magnetic and transport properties of Mn_3Ga thin films on Ta/Ru seed layer, J. Appl. Phys. 123 (2018) 103902.

[18] J.F. Qian, A.K. Nayak, G. Kreiner, W. Schnelle and C. Felser, Exchange bias up to room temperature in antiferromagnetic hexagonal Mn_3Ge, J. Phys. D: Appl. Phys. 47 (2014) 305001.

[19] A. Markou, J.M. Taylor, A. Kalache, P. Werner, S.S.P. Parkin and C. Felser, Noncollinear antiferromagnetic Mn_3Sn films, Phys. Rev. Materials 2 (2018) 051001(R).

[20] S. Tomiyoshi, Polarized Neutron Diffraction Study of the Spin Structure of Mn_3Sn. J. Phys. Soc. Jpn. 51 (1982) 803-810.

[21] A. Stroppa, M. Peressi, Non-collinear magnetic states of Mn_5Ge_3 compound. Mater. Sci. Semicond. Process. 9 (2006) 841–847.